nutrients

MDPI

Article

A Novel Polysaccharide (ZJP-2) from Wild Jujube Alleviates Oxidative Damage in Neural Stem Cells: Structural Features and Bioactivity

Shilan Li [1], Qiting Zhang [2], Jixian Liu [1], Xuchen Zhou [1], Ning Wang [1], Huabiao Chen [3], Nuermaimaiti Abudukelimu [4], Munisa Dilixiati [4], Xing Zhang [1,*] and Xinmin Liu [1,*]

[1] Zhejiang-Pakistan Joint Laboratory on R&D of Herbal Medicines, Institute of Drug Discovery and Technology, Ningbo University, Ningbo 315211, China
[2] Department of Chemical Biology, College of Chemistry and Chemical Engineering, Xiamen University, Xiamen 361005, China
[3] Health BioMed Co., Ltd., Ningbo 315042, China
[4] Xinjiang Technical Institute of Physics & Chemistry, Chinese Academy of Sciences, Urumqi 830063, China
* Correspondence: zhangxing@nbu.edu.cn (X.Z.); liuxinmin@nbu.edu.cn (X.L.)

Abstract

Background: Traditionally, wild jujube (*Ziziphus jujuba Mill. var. spinosa* (Bunge) Hu ex H. F. Chou) has been used to nourish the heart, calm the spirit, and arrest spontaneous sweating. Modern research confirms its broad pharmacological activities, including antioxidant, anti-inflammatory, neuroprotective, and cognitive-enhancing effects. This study aims to isolate and characterize the structure of jujube polysaccharides and evaluate their protective effects against oxidative stress damage in neural stem cells (NSCs). Methods: We successfully isolated and purified a novel pectin polysaccharide (ZJP-2) from wild jujube. Its structure was characterized in detail using high-performance liquid chromatography coupled with multi-angle laser light scattering and refractive index detection (HPLC-MALS-RI), high-performance anion exchange chromatography (HPAEC), gas chromatography–mass spectrometry (GC-MS), and nuclear magnetic resonance (NMR) spectroscopy. Results: Structural analysis revealed that ZJP-2 is a pectin heteropolysaccharide with a molecular weight of approximately 67.93 kDa. Its monosaccharide composition primarily includes galac-turonic acid (GalA), arabinose (Ara), rhamnose (Rha), galactose (Gal), and glucose (Glc). The backbone consists of α-GalA and rhamnose-galacturonic acid-I (RG-I) domains linked by (1→4)-glycosidic bonds. NMR spectroscopy further confirmed its glycosidic bond types. In activity assessment, our study demonstrated that ZJP-2 significantly alleviated DMNQ-induced oxidative stress damage in C17.2 neural stem cells. Its protective effect was achieved by reducing intracellular reactive oxygen species (ROS) levels and upregulating the mRNA expression of antioxidant genes associated with the signaling axis ($p < 0.05$). Moreover, ZJP-2 suppressed DMNQ-induced overexpression of Nestin and NeuN ($p < 0.05$), contributing to the maintenance of NSCs' undifferentiated state and functional homeostasis. Conclusions: In conclusion, ZJP-2 possesses distinct structural characteristics and significant neuroprotective potential, supporting its development as a natural functional food or dietary supplement for preventing oxidative stress-related neural damage.

Keywords: wild jujube; pectic polysaccharide; structural characterization; antioxidant activity; neuroprotective effect

Academic Editor: Peter Chi Keung Cheung

Received: 17 January 2026
Revised: 11 February 2026
Accepted: 24 February 2026
Published: 2 March 2026

1. Introduction

Natural bioactive compounds with dual food and medicinal properties have emerged as a significant global research focus for chronic disease prevention and overall health promotion, owing to their natural origins, high safety profile, and multi-targeted activities [1]. *Ziziphus jujuba Mill. var. spinosa*, an ancient Chinese medicinal and edible plant with over 8000 years of documented use [2], holds exceptional research value. Its mature seeds (Ziziphus jujuba seeds) serve as a core sedative agent in traditional Chinese medicine, renowned for their calming, tranquilizing, and heart-nourishing effects. Modern pharmacological studies further confirm these properties. Its research value is exceptionally high. Modern pharmacological studies have also extensively confirmed the broad potential of Ziziphus jujuba and its active components, including antioxidant, sedative-hypnotic, antidepressant, anxiolytic, and cognitive-enhancing properties [3–6]. However, despite its immense utility, wild jujube utilization faces structural limitations. Applications primarily focus on medicinal seeds (Ziziphus jujuba seeds, rich in saponins and flavonoids) and edible fruit peels, while the fruit pulp (non-medicinal or inedible portion) remains largely underutilized [7].

Given the underutilization of wild jujube pulp resources and the recognized potential of natural polysaccharides as biomacromolecules with outstanding antioxidant and immunomodulatory functions [8], their exploration warrants further investigation. Wild jujube polysaccharides (ZJPs) represent one of the abundant macromolecules in wild jujube pulp, exhibiting multiple biological activities [9]. Existing reports have confirmed that the monosaccharide composition of ZJPs includes rhamnose, glucose, arabinose, glucuronic acid, galactose, and xylose [9,10]. Regarding biological activity, related studies indicate that ZJPs possess antioxidant activity and immunomodulatory effects [11]. For instance, previous research demonstrated that ZJPs protect against experimental inflammatory bowel disease by enhancing intestinal barrier function [12]. Additionally, acidic heteropolysaccharides like PWJS have been shown to exhibit significant hepatoprotective effects [10]. Furthermore, although studies on ZJPs themselves remain relatively scarce, extensive research on Ziziphus genus polysaccharides has confirmed their multifaceted pharmacological activities, including antioxidant, anti-inflammatory, immunomodulatory, hypoglycemic, tumor growth inhibitory, and gastrointestinal-protective effects [13]. However, regarding structural elucidation, detailed structural or conformational information on Ziziphus jujuba polysaccharides remains extremely limited [11].

In summary, two major gaps exist in current research: first, structural studies largely remain at the level of simple component analysis, lacking in-depth structural elucidation of ZJPs; second, systematic research on the neuroprotective mechanisms of Ziziphus jujuba polysaccharides, or even Ziziphus genus polysaccharides, is absent. This study aims to address these gaps in structural and functional research and advance the comprehensive utilization of Ziziphus jujuba fruit pulp resources. We have successfully isolated and purified a novel pectin polysaccharide from wild jujube pulp, designated ZJP-2. To precisely determine its chemical structure and structural novelty, this study employed a series of advanced techniques including HPLC-MALS-RI, HPAEC, GC-MS, and NMR to systematically characterize the structural features of ZJP-2. Subsequently, we evaluated the neuroprotective potential of ZJP-2 using a DMNQ-induced oxidative stress model in C17.2 neural stem cells. This research will provide theoretical support for the application of wild jujube in functional foods and the treatment of central nervous system disorders, while establishing a scientific foundation for enhancing the comprehensive utilization of wild jujube resources.

2. Materials and Methods

2.1. Chemicals and Reagents

Sodium nitrate (analytical reagent grade, AR) was purchased from Sinopharm Chemical Reagent Co., Ltd. (Shanghai, China). Methanol was obtained from ANPEL Laboratory Technologies Inc. (Shanghai, China). Sodium hydroxide, sodium acetate trihydrate, dimethyl sulfoxide (DMSO), sodium borodeuteride ($NaBD_4$), and acetic anhydride were purchased from Sigma-Aldrich (St. Louis, MO, USA). Trifluoroacetic acid (TFA), acetic acid, and dichloromethane (DCM) were obtained from CNW Technologies GmbH (Düsseldorf, Germany). Ultrapure water was prepared in-house using a Milli-Q water purification system (Millipore, Bedford, MA, USA).

2.2. Extraction and Purification of ZJP-2

Fresh fruits of *Ziziphus jujuba* Mill. var. *spinosa* were harvested from Toksun County, Xinjiang Uygur Autonomous Region, China. The fruits were de-seeded, freeze-dried, ground into powder, and passed through a 60-mesh sieve. The resulting powder was extracted twice with ultrapure water (solid-to-liquid ratio of 1:20, *w*/*v*) at 85 °C for 2 h per extraction. The extracts were centrifuged to collect the supernatant, which was concentrated under reduced pressure. Four volumes of ethanol were added to precipitate the polysaccharides overnight. The precipitate was collected, redissolved in water, and freeze-dried to yield crude wild jujube polysaccharides.

The crude polysaccharides were resuspended in ultrapure water and purified using a DEAE-650M ion-exchange chromatography column (6 × 20 cm, Tosoh Corporation, Tokyo, Japan). The column was eluted sequentially with ultrapure water and 0.4 M NaCl solution. The fraction eluted with ultrapure water was collected and freeze-dried to obtain the neutral polysaccharide ZJP-1. The fraction eluted with 0.4 M NaCl solution was dialyzed against ultrapure water for 48 h (MWCO 3.5 kDa, Solarbio Science & Technology, Beijing, China). The fraction retained in the dialysis bag was freeze-dried to obtain the acidic polysaccharide ZJP-2.

2.3. Structural Analysis of Polysaccharides

2.3.1. Molecular Weight Determination of Polysaccharides

The homogeneity and molecular weight of ZJP-2 were determined using HPLC-MALS-RI [14]. The specific conditions were as follows: a DAWN HELEOS-II laser photometer (Wyatt Technology, Santa Barbara, CA, USA) equipped with two tandem columns (300 × 8 mm, Shodex OH-pak SB-805 and 803; Showa Denko K.K., Tokyo, Japan) was maintained at 45 °C using a column heater model by Sanshu Biotech Co., Ltd. (Shanghai, China). Additionally, a differential refractive index detector (Optilab T-rEX, Wyatt Technology, Santa Barbara, CA, USA) measured the concentration and dn/dc value of each component. The dn/dc value of the fractions was determined to be 0.141 mL/g. ASTRA software (Version 6.1, Wyatt Technology, Santa Barbara, CA, USA) facilitated the acquisition and subsequent processing of all data. This analysis yielded quantitative results for parameters such as the number-average molecular weight *(Mn)*, the weight-average molecular weight (*Mw*), and the polydispersity index (*Mw*/*Mn*).

2.3.2. Monosaccharide Compositions

The monosaccharide composition of ZJP-2 was determined by high-performance anion-exchange chromatography with pulsed amperometric detection (HPAEC-PAD) [15]. The analysis was performed on a Dionex ICS-5000+ system (Thermo Scientific, Waltham, MA, USA) equipped with a CarboPac PA-20 column (3 × 150 mm). The mobile phases consisted of (A) ultrapure water, (B) 0.1 M NaOH, and (C) 0.1 M NaOH containing 0.2 M

NaAc. The flow rate was set at 0.5 mL/min with an injection volume of 5 μL. The gradient elution program was applied as follows: 0 min, 95% A, 5% B; 26–42 min, 85% A, 5% B, 10% C; 42.1 min, 60% A, 40% C; 52 min, 60% A, 40% B; 52.1–60 min, 95% A, 5% B for re-equilibration. Data acquisition and processing were performed using Chromeleon 7.2 CDS software (Version 7.2, Thermo Fisher Scientific, Waltham, MA, USA).

2.3.3. Methylation Analysis of ZJP-2

Since ZJP-2 contains uronic acids, carboxyl reduction was performed prior to methylation to convert uronic acids into their corresponding neutral sugars according to the method of Taylor and Conrad [16] with minor modifications. Briefly, the sample (5 mg) was dissolved in water and reacted with 1-cyclohexyl-3-(2-morpholinoethyl) carbodiimide metho-p-toluenesulfonate (CMC) for 2 h. The solution was then divided into two parts and reduced with $NaBH_4$ and $NaBD_4$, respectively, to distinguish the original neutral sugars from the reduced uronic acids.

Subsequently, the reduced polysaccharide was methylated using the Ciucanu and Kerek method [17]. The sample was dissolved in DMSO (500 μL) and incubated with NaOH powder for 30 min, followed by reaction with me thyl iodide (CH_3I) for 1 h. The methylated products were extracted with dichloromethane. Finally, the samples were hydrolyzed with 2 M TFA at 121 °C for 90 min, reduced with $NaBD_4$, and acetylated with acetic anhydride to yield partially methylated alditol acetates (PMAAs). The PMAAs were analyzed by GC-MS (Agilent Technologies, Santa Clara, CA, USA).

2.3.4. Nuclear Magnetic Resonance (NMR) Spectroscopy

The purified polysaccharide ZJP-2 (20 mg) was dissolved in 0.5 mL of deuterium oxide (D_2O, 99.9%). NMR spectra, including ^1H, ^{13}C, ^1H-^1H COSY, HSQC, and HMBC, were acquired using a Bruker AVANCE NEO 600 MHz spectrometer (Bruker BioSpin GmbH, Rheinstetten, Germany) at 298 K.The experimental parameters were set as follows: the number of scans (NS) was 64 for ^1H NMR and 13,921 for ^{13}C NMR to ensure sufficient signal-to-noise ratio. For 2D NMR spectra, the number of scans was set to 128 for HSQC and 160 for HMBC. Chemical shifts (δ) are expressed in ppm relative to the solvent peak (HDO, δ 4.79 ppm). Data processing was performed using MestReNova software [18] (Version 14.2, Mestrelab Research, Santiago de Compostela, Spain).

2.4. Protective Effect on Nerve Cells

2.4.1. Cell Culture

The C17.2 neural stem cell line was procured from OriCell (Shanghai, China). The cells were cultured in proliferation medium formulated according to the method of Li et al. with slight modifications [19]. The growth medium consisted of high-glucose Dulbecco's Modified Eagle Medium (DMEM; Gibco, Grand Island, NY, USA) supplemented with 10% fetal bovine serum (FBS; Gibco, Grand Island, NY, USA) and 5% horse serum (HS; Gibco, Grand Island, NY, USA). The cultures were maintained in a humidified incubator (Thermo Fisher Scientific, Waltham, MA, USA) at 37 °C with a 5% CO_2 atmosphere. Cells were passaged when they reached 70–80% confluence.

2.4.2. Cell Viability Assessment (CCK-8 Assay)

C17.2 cells were seeded at a density of 5×10^3 cells in 96-well plates containing proliferation medium and cultured for 24 h. Subsequently, cells were treated with DMNQ at various concentrations (0, 1, 3, 6, 9, 12, 24 μM) for 24 h. Concurrently, an equal volume of DMSO (0.1%) served as the solvent control. Cell viability was assessed using the CCK-8 assay kit (Beyotime Biotechnology, Shanghai, China) [20]. The procedure was carried out according to the manufacturer's instructions. The absorbance was measured at 450 nm

using a microplate reader (Molecular Devices, San Jose, CA, USA), Country])Cell viability was then calculated using the following formula: Cell viability (%) = Mean absorbance of treated group/Absorbance of control group × 100%.

C17.2 cells were seeded at a density of 5 × 10^3 cells per well in a 96-well plate containing proliferation medium and cultured for 24 h. A DMNQ concentration of 3 μM was used for subsequent experiments. ZJP-2 (400 μg/mL) and DMNQ (3 μM) were added to the C17.2 cells and incubated together for 24 h. Cell viability was then tested by CCK-8 assay.

2.4.3. Flow Cytometry Analysis

C17.2 cells were seeded at a density of 1 × 10^5 cells per well in 6-well plates and cultured for 24 h. The cells were then treated with DMNQ (3 μM) alone or co-treated with DMNQ (3 μM) and ZJP-2 (400 μg/mL) for 24 h. After treatment, the cells were harvested, washed with PBS, and stained using the Annexin V-FITC/PI Apoptosis Detection Kit (A026, GeneCopoeia, Rockville, MD, USA) according to the manufacturer's protocol. Finally, the percentage of apoptotic cells was analyzed using a BD FACSCanto™ II Flow Cytometer (BD Biosciences, San Jose, CA, USA), and data processing was performed using BD FACSDiva software (Version 8.0, BD Biosciences, San Jose, CA, USA).

2.4.4. ROS Detection

Intracellular ROS levels were assessed using the CellROX™ Deep Red Reagent (Thermo Fisher Scientific, Waltham, MA, USA) following a previously described method [21]. Briefly, C17.2 cells were treated with DMNQ (3 μM) alone or co-treated with ZJP-2 (400 μg/mL) for 24 h. Subsequently, the cells were stained with 10 μM CellROX™ Deep Red and incubated at 37 °C in the dark for 30 min. After incubation, the cells were washed with PBS, harvested, and resuspended. The mean fluorescence intensity (MFI) was analyzed using flow cytometry (BD Biosciences, San Jose, CA, USA), and data processing was performed using BD FACSDiva software (Version 8.0, BD Biosciences, San Jose, CA, USA).

2.4.5. Real-Time qPCR Analysis

Total RNA [22] was extracted using the E.Z.N.A.® Total RNA Kit I (Omega Biotek, Norcross, GA, USA) according to the manufacturer's instructions. The purity and concentration of RNA were assessed using a NanoDrop 1000 spectrophotometer (Thermo Fisher Scientific). First-strand cDNA was synthesized using the gDNA Digester Plus kit (Yeasen Biotechnology, Shanghai, China) following the manufacturer's protocol.

mRNA expression levels were determined by RT-qPCR using the Hieff® qPCR SYBR® Green Master Mix (Yeasen Biotechnology, Shanghai, China) on a CFX96 Real-Time PCR Detection System (Bio-Rad, Hercules, CA, USA). The reaction mixture (20 μL) contained 2 μL of cDNA, 0.4 μL of each primer (10 μM), 10 μL of Master Mix, and 7.2 μL of nuclease-free water. The cycling conditions were as follows: initial denaturation at 95 °C for 5 min, followed by 40 cycles of denaturation at 95 °C for 10 s, annealing at 60 °C for 20 s, and extension at 72 °C for 20 s. A melting curve analysis was performed using the instrument's default settings. All samples were analyzed in duplicate, and GAPDH was used as the internal control. The primer sequences employed in the experiment are as follows: *HO-1* (NM_010442.2): forward primer is AAGCCGAGAATGCTGAGTTCA, the reverse primer is GCCGTGTAGATATGGTACAAGGA; *NRF-2* (NM_010938.4): forward primer is TCACAGAGAGAGGGAAAAGGCC, the reverse primer is GCAGGGGCCAACCTCTGTCG; *SOD1* (NM_000454): forward primer is GGTGTGCGTGCTGAAAGAG, the reverse primer is CAGGTCTCCAACATGCCTCT; *GAPDH* (NM_001289726.1): forward primer is GCACAGTCAAGGCCGAGAAT, the reverse primer is GCCTTCTCCATGGTGGTGAA.

2.4.6. Western Blot Analysis

The protein expression levels of Nestin and NeuN were analyzed via Western blot [23]. Total protein (15 μg) was separated by 12.5% SDS-PAGE and transferred onto PVDF membranes (Millipore, Billerica, MA, USA). The membranes were blocked with 5% skimmed milk at 4 °C for 30 min. Subsequently, the membranes were incubated with primary antibodies against Nestin (1:1000; Proteintech, Rosemont, IL, USA; Cat. No. 19483-1-AP) and NeuN (1:20,000; Proteintech; Cat. No. 26975-1-AP) overnight at 4 °C. After washing, the membranes were incubated with HRP-conjugated secondary antibodies (1:10,000; Proteintech; Cat. No. SA00001-2) at room temperature for 1 h. Target protein bands were visualized using an ECL kit (GE Healthcare, Chicago, IL, USA) and imaged using a ChemiDoc Imaging System (Bio-Rad, Hercules, CA, USA). Protein band intensities were quantified using ImageJ software (version 1.51m9, NIH, Bethesda, MD, USA).

2.5. Statistical Analysis

All statistical analyses were performed using GraphPad Prism 9.0 software (GraphPad Software, La Jolla, CA, USA). Data are expressed as the mean ± standard error of the mean (SEM). Differences between two groups were analyzed using Student's *t*-test. Multiple group comparisons were analyzed using one-way analysis of variance (ANOVA) followed by Tukey's post hoc test (or Dunnett's test). A *p*-value of less than 0.05 ($p < 0.05$) was considered statistically significant.

3. Results

3.1. Isolation and Purification of ZJP-2

Wild jujube pulp was crushed and subjected to reflux extraction with hot deionized water for crude extraction. Ethanol precipitation yielded crude wild jujube polysaccharides. The crude polysaccharide sample was redissolved in water and separated using a DEAE-650M ion exchange column (6 × 20 cm). The column was first eluted with ultrapure water to obtain ZJP-1, followed by elution with ultrapure water and 0.4 M NaCl solution to collect the acidic polysaccharide fraction. This acidic fraction underwent dialysis with a molecular weight cutoff of 3.5 kDa against ultrapure water to remove small-molecule impurities and salts, ultimately yielding the target product—novel Ziziphus jujuba pectin polysaccharide designated as ZJP-2—after freeze-drying. This product was used for subsequent further analysis.

3.2. Molecular Weight and Homogeneity of ZJP-2

The molecular weight of polysaccharides plays a crucial role in determining their biological activity [13]. The homogeneity and molecular weight distribution of ZJP-2 were evaluated by HPLC-MALS-RI (Figure 1A). The light scattering (LS) signal exhibited a single dominant peak at approximately 20 min, indicating the presence of a high-molecular-weight fraction. The refractive index (RI) detector displayed a major peak at 25 min with a minor shoulder at ~35 min, which showed negligible LS response, suggesting trace low-molecular-weight impurities or partial degradation products that do not influence the characterization of the main component. The weight-average molecular weight (*Mw*) of ZJP-2 was 6.79×10^4 Da, with a polydispersity index (*Mw*/*Mn*) of 2.5 (Table S1), reflecting the moderate heterogeneity typical of natural pectic polysaccharides [24].

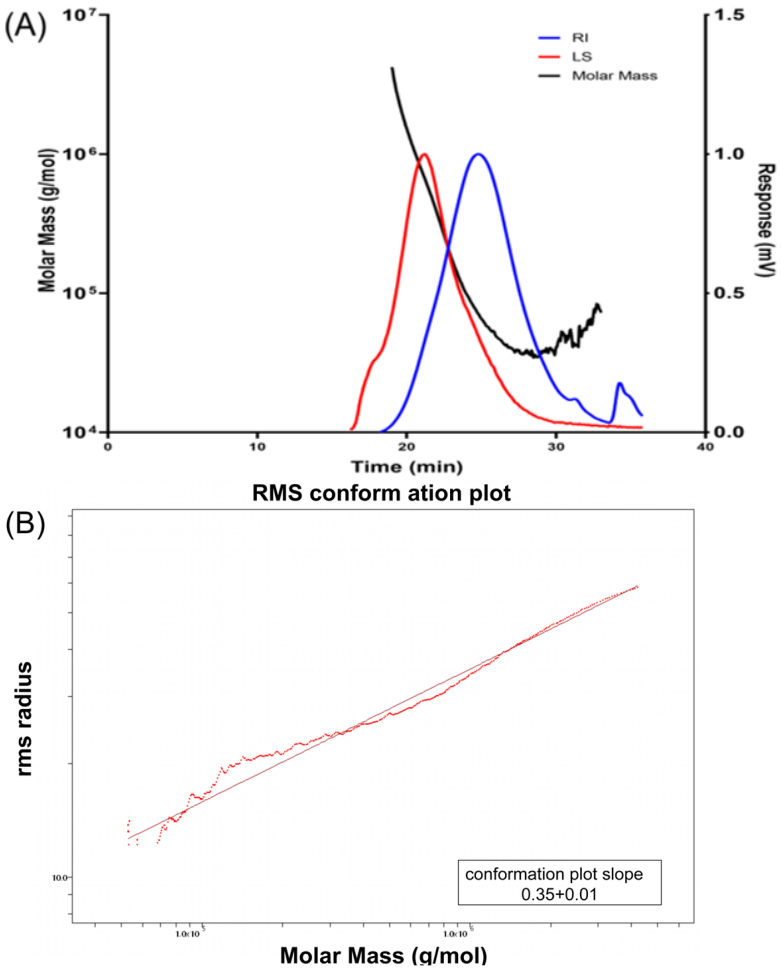

Figure 1. Average molecular weight of ZJP-2 obtained from HPLC-MALS-RI. (**A**) Average molecular weight; (**B**) root-mean-square (RMS) radius conformation plot.

To further assess its molecular conformation in aqueous solution, a log-log plot of the root-mean-square (R.M.S.) radius versus molecular weight was constructed (Figure 1B). The slope of the linear fit was 0.35 ± 0.01, indicating a compact, nearly spherical conformation in solution [25]. This compact architecture is consistent with plant-derived pectic polysaccharides and has been associated with favorable solubility, structural stability, and potential bioactivity [26].

3.3. Monosaccharide Composition Analysis

Monosaccharide composition analysis was carried out using ion chromatography [15]. As shown in Figure 2, ZJP-2 primarily consisted of galacturonic acid (GalA), arabinose (Ara), rhamnose (Rha), galactose (Gal), and glucose (Glc), in a molar ratio of approximately 7.81:6.83:2.73:2.59:1.00 (Table S2), corresponding to molar percentages of 37.26%, 32.59%, 13.02%, 12.36%, and 4.77%, respectively. Combined with the molecular weight (67.93 kDa), these results indicate that ZJP-2 is an acidic heteropolysaccharide with a moderate molecular weight [13]. The high content of galacturonic acid, along with characteristic pectic monosaccharides such as arabinose and rhamnose, suggests that ZJP-2 may belong to the pectic polysaccharide family [27]. The presence of galactose and glucose further indicates the possible existence of neutral sugar domains or heteropolysaccharides features.

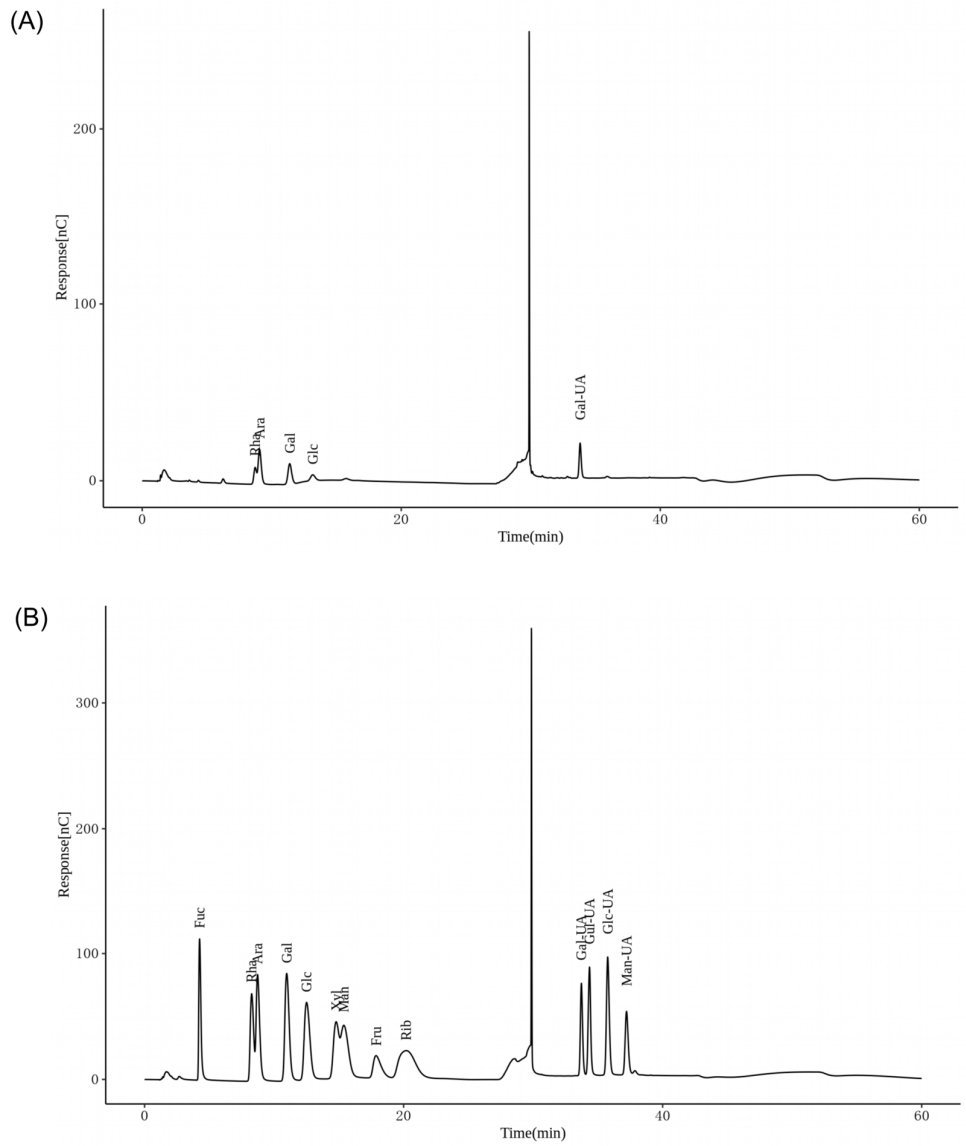

Figure 2. HPAEC-PAD chromatograms of (**A**) hydrolyzed ZJP-2 and (**B**) mixed monosaccharide standards.

These structural traits provide a valuable foundation for the in-depth investigation of its structure–activity relationship and potential functional applications. For instance, a polysaccharide isolated from *Ziziphus jujuba cv. Muzao* was also reported to primarily contain GalA (42.78%), Ara (25.12%), Rha (13.31%), and Gal (11.45%) as major components. This is consistent with a typical pectic structure featuring HG and RG-I regions [28]. Similarly, another study identified a wild jujube polysaccharide with a molar ratio of GalA: Ara: Rha: Gal close to 5.6:3.7:2.2:2.0, highlighting a comparable acidic and branched sugar profile with ZJP-2 [29]. These findings indicate that ZJP-2 shares similar structural features with other known pectic polysaccharides from wild jujube, further supporting its classification within the pectic-type family and its potential for immunomodulatory or antioxidant applications.

3.4. Methylation Analysis

Methylation analysis was performed to elucidate the glycosidic linkage patterns of ZJP-2 [30]. The primary linkage types are summarized in Table 1. The results revealed that ZJP-2 is composed of diverse sugar residues. The most abundant residue was 1,4-linked

Gal*p*A (32.13%), followed by 1,4-linked Gal*p* (17.79%), 1,5-linked Ara*f* (8.71%), and 1,2,4-linked Rha*p* (8.31%). Specifically, the high proportion of 1,4-linked Gal*p*A, along with minor amounts of 1,3,4-linked Gal*p*A (2.37%), confirmed the presence of a homogalacturonan (HG) backbone [31,32]. The detection of 1,2-linked Rha*p* (6.19%) and branched 1,2,4-linked Rha*p* (8.31%) residues indicated the existence of rhamnogalacturonan-I (RG-I) regions, where the O-4 position of rhamnose serves as the attachment point for side chains [33]. Regarding the side chains, arabinose residues were primarily present as terminal Ara*f* (7.87%), 1,5-linked Ara*f* (8.71%), and branched 1,2,5-linked Ara*f* (1.72%), suggesting the presence of arabinan or arabinogalactan side chains. Galactose residues mainly existed as 1,4-linked Gal*p* (17.79%) and branched 1,3,6-linked Gal*p* (1.96%), further supporting the complexity of the neutral side chains [34]. Additionally, minor amounts of glucose residues (1,4-linked and 1,2,4-linked Glc*p*) were detected, likely representing amorphous regions or short heteropolysaccharide chains.

Table 1. Methylation analysis data of ZJP-2.

Peak No	Retention Time (min)	Methylated Sugars	Linkage Patterns	Molar Ratio (%)
1	7.760	1,4-di-O-acetyl-2,3,5-tri-O-methyl arabinitol	t-Ara*f*	7.87
2	8.404	1,5-di-O-acetyl-6-deoxy-2,3,4-tri-O-methyl rhamnitol	t-Rha*p*	1.11
3	9.214	1,5-di-O-acetyl-2,3,4-tri-O-methyl arabinitol	t-Ara*p*	1.25
4	12.762	1,2,5-tri-O-acetyl-6-deoxy-3,4-di-O-methyl rhamnitol	2-Rha*p*	6.19
5	12.892	1,5-di-O-acetyl-2,3,4,6-tetra-O-methyl galactitol	t-Gal*p*A	7.21
6	13.479	1,4,5-tri-O-acetyl-2,3-di-O-methyl arabinitol	5-Ara*f*	8.71
7	17.235	1,2,4,5-tetra-O-acetyl-6-deoxy-3-O-methyl rhamnitol	2,4-Rha*p*	8.31
8	17.592	1,4,5-tri-O-acetyl-2,3,6-tri-O-methyl galactitol	4-Gal*p*	17.79
9	17.668	1,4,5-tri-O-acetyl-2,3,6-tri-O-methyl galactitol	4-Gal*p*A	32.13
10	17.905	1,4,5-tri-O-acetyl-2,3,6-tri-O-methyl glucitol	4-Glc*p*	1.80
11	18.054	1,2,4,5-tetra-O-acetyl-3-O-methyl arabinitol	2,5-Ara*f*	1.72
12	20.065	1,3,4,5-tetra-O-acetyl-2,6-di-O-methyl galactitol	3,4-Gal*p*A	2.37
13	21.668	1,2,4,5-tetra-O-acetyl-3,6-di-O-methyl glucitol	2,4-Glc*p*	1.58
14	24.045	1,3,5,6-tetra-O-acetyl-2,4-di-O-methyl galactitol	3,6-Gal*p*	1.96

Collectively, these methylation results are highly consistent with the monosaccharide composition data. The dominance of 1,4-linked Gal*p*A corresponds well with the high content of galacturonic acid (37.26%) observed in HPAEC analysis. Similarly, the abundance of arabinose (terminal and 1,5-linked) and galactose (1,4-linked) residues aligns perfectly with their high molar percentages in the monosaccharide composition. These results confirm that ZJP-2 is a pectic-type acidic heteropolysaccharide characterized by an HG and RG-I backbone substituted with arabinan and galactan side chains [35]. This structural model aligns with previous studies on wild jujube polysaccharides. For instance, the polysaccharide DPZMP4 from *Ziziphus jujuba cv. Muzao* was shown to possess a 1,4-linked Gal*p*A backbone branched with Ara*f* and Gal*p* residues [36]. Similarly, the pectic polysaccharide SAZMP4 was found to contain an HG backbone with RG-I-type side chains comprising 1-linked Ara*f*, 1,2,4-linked Rha*p*, and 1,4-linked Gal*p* [37].

The linkage patterns observed in ZJP-2 may contribute significantly to its biological functions. Polysaccharides featuring a backbone rich in 1→4 linked GalA and RG-I domains with arabinose-rich side chains have been reported to exhibit potent antioxidant activities, including free radical scavenging and metal ion chelation [38]. The high content of unmethylated uronic acids and the complex branched architecture of ZJP-2 likely provide the structural basis for its antioxidant potential observed in this study.

3.5. NMR Analysis

The chemical structure of ZJP-2, including the chemical shifts and glycosidic linkage sequence for individual sugar residues, was elucidated through Nuclear Magnetic Resonance (NMR) spectroscopy. As presented in the ^{1}H NMR spectrum (Figure 3A), the vast

number of proton signals was located within δ_H 3.0–5.5 ppm. This broad distribution suggests the presence of multiple distinct sugar residues within the polysaccharide structure. Specifically, some coupled signal peaks were discernable in the anomeric region spanning δ_H 4.3–5.4 ppm. The most prominent anomeric proton signals were observed δ_H 4.49, 4.94, 5.06, 5.09, 5.12, 5.15, 5.21, and 5.25, respectively. Ten distinct anomeric carbon signals are observed in the ^{13}C NMR spectrum (Figure 3B), with chemical shifts corresponding to δ_C 109.2, 107.4, 107.0, 104.4, 103.2, 100.4, 99.5, 98.5, 98.3, and 97.4, respectively. The chemical shifts at 1.28 ppm and 1.22 ppm are hydrogen signals from the -CH3 group on rhamnose; the chemical shift at 3.78 ppm is a hydrogen signal from the -OCH3 group, which correlates with the chemical shift of 52.8 ppm in the C spectrum. The chemical shifts at 170.6 ppm and 174.0/175.1 ppm in the ^{13}C NMR spectrum (Figure 3B) are carbonyl signals from the methyl ester and carboxylic acid groups, respectively, on the sugar residues of ZJP-2. Furthermore, to precisely assign these anomeric signals, we performed a joint analysis of the cross-peaks in the anomeric region of the spectrum (Figure 3A), ^{13}C NMR spectrum (Figure 3B), and HSQC spectrum (Figure 3C). Through this combined analysis, we successfully determined the values corresponding to the cross-peaks in the sample: $\delta_{H/C}$ 5.12/107.0, 5.06/107.4, 5.21/109.2, 5.25/97.4, 5.15/98.3, 5.06/103.2, 5.06/98.5, 4.88/99.5, 4.94/100.4, and 5.09/104.4. Subsequently, these signals were named residues A, B, D, E, F, G, I, J, K, and L, based on their chemical shift characteristics (Figure 3F). To clarify the structure, the spin systems of these residues are discussed separately, followed by the linkage analysis.

According to the analysis of monosaccharide composition and methylation, and in combination with the relevant signals of HSQC spectrum (Figure 3C) and ^{1}H-^{1}H COSY spectrum (Figure 3D), and combined with previous literature reports [39–41], we attributed the various signals of sugar residues. Two rhamnose residues were identified by their characteristic methyl group signals (H-6) at δ_H1.22 and 1.28 ppm in the high-field region. Residue E (δ_H 5.25/δ_C 97.4) was assigned as (1→2)-α-L-Rha*p*. Residue F (δ_H 5.15/δ_C 98.3) exhibited downfield shifts at *C*-2 and *C*-4, indicating that it serves as a branching point, assigned as (1→2,4)-α-L-Rha*p*. Signals for galacturonic acid were distinguished by carboxyl carbon signals (δ_C 170.6 and 175.1 ppm). Residue L (δ_H 5.09/δ_C 104.4) showed a correlation with a methoxy proton signal (δ_H 3.78/δ_C 52.8), confirming it as a methyl-esterified (1→4)-α-D-Gal*p*A-6-OMe. Residue J (δ_H 4.88/δ_C 99.5) and Residue K (δ_H 4.94/δ_C 100.4) were assigned as terminal α-D-Gal*p*A and branched (1→3,4)-α-D-Gal*p*A, respectively. Three arabinose residues were identified by their anomeric carbon shifts in the downfield (>107 ppm), characteristic of furanose rings. Residue A (δ_H 5.12/δ_C 107.0) was assigned as terminal α-L-Ara*f*. Residue B (δ_H 5.06/δ_C 107.4) and Residue D (δH 5.21/δC 109.2) were assigned as (1→5)-α-L-Ara*f* and (1→2,5)-α-L-Ara*f*, respectively. Based on literature values and chemical shifts, Residue G (δ_H 5.06/δ_C 103.2) was attributed to (1→4)-α-D-Gal*p*, and Residue I (δ_H 5.06/δ_C 98.5) was attributed to (1→4)-α-D-Glc*p*. The chemical signal shifts in each sugar residue in ZJP-2 are summarized in Table 2. Generally, the α-configuration was assigned based on the anomeric proton chemical shifts (>4.8 ppm) in combination with the literature data [42].

Methylation analysis indicated that ZJP-2 possesses a backbone composed of alternating (1→4)-α-D-Gal*p*A and (1→2,4)-α-L-Rha*p* units, a characteristic feature of Rhamnogalacturonan-I (RG-I) pectins. Additionally, the presence of (1→4)-D-Gal*p* and (1→5)-L-Ara*f* linkages suggests the existence of linear galactan and arabinan side chains attached to the O-4 position of rhamnose residues [43,44]. The glycosidic linkages and sequence of ZJP-2 were determined by analyzing the long-range correlations in the HMBC spectrum (Figure 3E). The RG-I backbone consists of alternating GalA and Rha residues. Strong cross-peaks were observed between H-1 of Residue L (GalA) and *C*-2 of Residues E/F (Rha) (δ_H 5.09/δ_C 76.5/76.6), and reciprocally between H-1 of Residues E/F (Rha)

and *C*-4 of Residue L (GalA) (δ_H 5.25/82.2; δ_H 5.15/82.2). This confirms the repeating unit: (1→4)-α-D-Gal*p*A-6-OMe-(1→2)-α-L-Rha*p*. The branching points were identified on the Rha and GalA residues. The cross-peaks of G H-1/F *C*-4 (δ_H 5.06/δ_C 79.0) and D H-1/F *C*-4 (δ_H 5.21/δ_C 79.0) indicated that neutral side chains (Galactan and Arabinan) are attached to the O-4 position of rhamnose (Residue F). Additionally, a correlation between K H-1/L *C*-4 (δ_H 4.94/δ_C 82.2) suggested linkages between GalA residues. The internal structure of the side chains was elucidated by correlations such as A H-1/B *C*-5 (δ_H 5.12/δ_C 66.4) and B H-1/D *C*-5 (δ_H 5.06/δ_C 66.8), confirming the sequence of arabinan side chains (Term-Ara→5-Ara→2,5-Ara). Similarly, L H-1/I *C*-4 (δ_H 5.09/δ_C 79.0) and I H-1/K *C*-3 (δ_H 5.06/δ_C 79.0) revealed the connection involving Glc residues. Based on the integration of methylation analysis, 1D/2D NMR data, and literature comparisons, the putative structural formula of ZJP-2 was proposed as shown in Figure 3F. This indicates that Residue B, Residue G, and Residue L were identified as major structural units of ZJP-2.

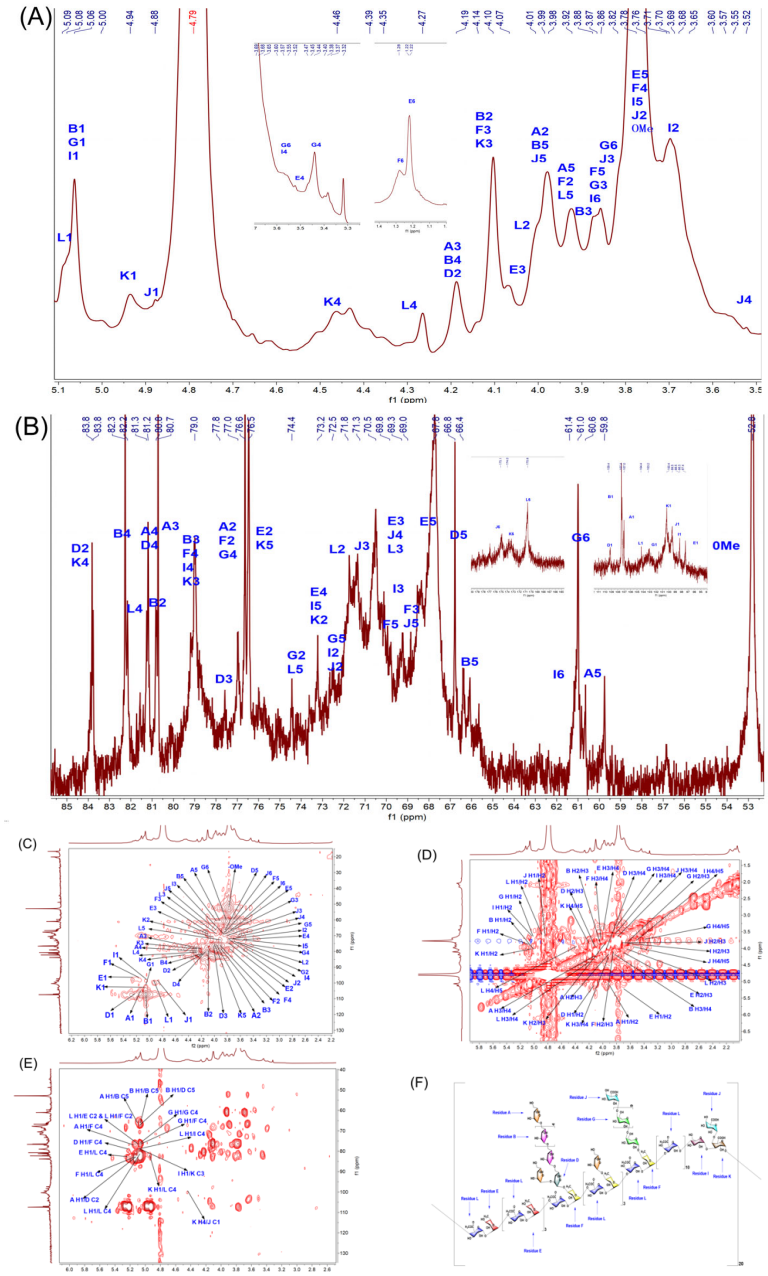

Figure 3. NMR spectral analysis of ZJP-2. (**A**) ^{1}H-NMR; (**B**) ^{13}C-NMR; (**C**) ^{1}H-^{1}H COSY; (**D**) HSQC; (**E**) HMBC; (**F**) proposed structural model of ZJP-2 based on NMR analysis.

Table 2. Assignments of ^{1}H and ^{13}C NMR spectra for ZJP-2.

Sugar Residues	Chemical Shifts δ (ppm)						-OMe
	H-1 *C*-1	H-2 *C*-2	H-3 *C*-3	H-4 *C*-4	H-5 *C*-5	H-6 *C*-6	
T α-L-Ara*f*	5.12	3.98	4.19	4.27	3.92/n.d	-/-	
Residue A	107.0	76.6	80.7	81.2	60.6	-/-	
(1→5)-α-L-Ara*f*	5.06	4.10	3.88	4.19	3.98/n.d	-/-	
Residue B	107.4	80.8	79.0	82.3	66.4	-/-	
(1→2,5)-α-L-Ara*f*	5.21	4.19	3.99	4.14	3.83/3.76	-/-	
Residue D	109.2	83.8	77.8	81.3	66.8	-/-	
(1→2)-α-L-Rha*p*	5.25	3.76	4.07	3.52	3.78	1.22	
Residue E	97.4	76.5	70.5	73.2	67.8	16.9	
(1→2,4)-α-L-Rha*p*	5.15	3.92	4.10	3.78	3.86	1.28	
Residue F	98.3	76.6	69.0	79.0	69.3	16.8	
(1→4)-α-D-Gal*p*	5.06	3.70	3.86	3.44	3.68	3.82/3.55	
Residue G	103.2	74.4	70.1	76.6	72.5	61.0	
(1→4)-α-D-Glc*p*	5.06	3.71	3.87	3.55	3.78	3.58/3.86	
Residue I	98.5	72.5	69.6	79.0	73.2	61.4	
T α-D-GalA*p*	4.88	3.78	3.82	3.60	3.98	/	
Residue J	99.5	72.5	71.3	70.5	69.0	175.1	
(1→3,4)-α-D-GalA*p*	4.94	3.68	4.10	4.46	3.99	-/-	
Residue K	100.4	73.2	79.0	83.8	76.5	174.1	
(1→4)-α-D-GalA*p*-6-OMe	5.09	4.01	3.99	4.27	3.92	-/-	3.78
Residue L	104.4	71.8	70.5	82.2	74.4	170.6	52.8

"n.d" indicates not determined, "-" indicates not applicable.

3.6. ZJP-2 Protect C17.2 Cells from DMNQ Injury

3.6.1. Cell Vitality and Apoptosis

To evaluate the cytotoxicity of ZJP-2, C17.2 neural stem cells were treated with various concentrations of ZJP-2 (200, 400, 600, 800, 1200, and 1600 μg/mL) for 24 h. As shown in Figure 4B, none of the tested concentrations significantly affected cell viability ($p > 0.05$), indicating that ZJP-2 is non-toxic within this concentration range. For further study, a concentration of 400 μg/mL was selected because it provided a balance between pharmacological efficacy and non-specific interference caused by high-dose exposure [45].

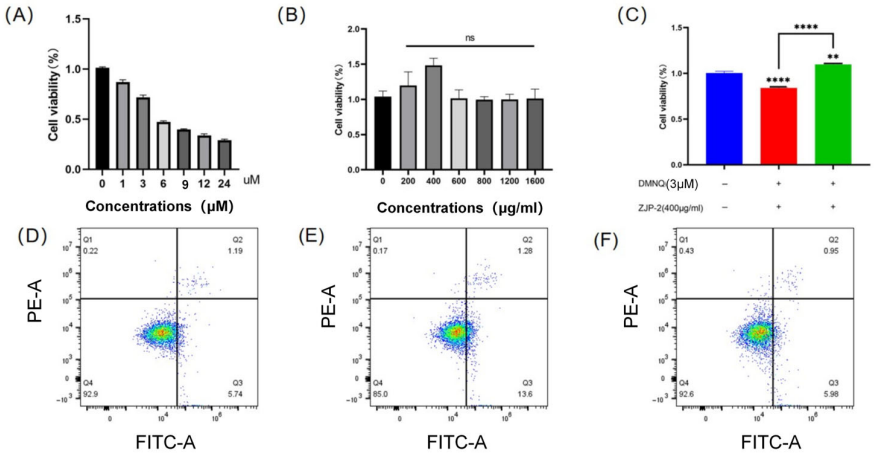

Figure 4. Protective effect of ZJP-2 on C17.2 cell viability and DMNQ-induced oxidative damage. (**A**) Effects of different concentrations of ZJP-2 on C17.2 cell viability after 24 h of treatment ($n = 6$). (**B**) Effects of different concentrations of DMNQ on C17.2 cell viability after 24 h of treatment ($n = 6$). (**C**) Protective effect of ZJP-2 (400 μg/mL) on 3 μM DMNQ-induced C17.2 cell damage ($n = 6$). (**D**–**F**) Representative flow cytometry plots showing the apoptotic rates of C17.2 cells in different groups: (**D**) Control group: cells cultured in normal medium; (**E**) Model group: cells treated with DMNQ (3 μM) alone for 24 h; (**F**) ZJP-2 group: cells co-treated with DMNQ (3 μM) and ZJP-2 (400 μg/mL) for 24 h. Data are expressed as mean ± SEM, ** $p < 0.01$, **** $p < 0.001$ vs. Control group (or Model group); ns indicates not significant. Statistical analysis was performed using one-way ANOVA followed by LSD test.

To establish an oxidative stress model, C17.2 cells were exposed to various concentrations of DMNQ for 24 h. DMNQ has been proven to induce oxidative stress primarily through redox cycling. During this process, DMNQ undergoes enzymatic one-electron reduction to form a semiquinone radical, which reacts with molecular oxygen to generate superoxide anions and other ROS [46]. This continuous ROS production disrupts redox homeostasis and causes oxidative damage in cellular components. Treatment with 3 μM of DMNQ reduced cell viability to approximately 70% (Figure 4A), and this concentration was thus chosen for the injury model (Figure 4A).

To evaluate the protective effects of ZJP-2, C17.2 cells were co-treated with DMNQ (3 μM) and ZJP-2 (400 μg/mL) for 24 h. As shown in Figure 4C, ZJP-2 significantly attenuated the cytotoxicity of DMNQ, restoring cell viability to levels comparable to the untreated control ($p < 0.05$). These findings suggest that ZJP-2 effectively protects the neural stem cells against oxidative stress-induced injury ($p < 0.05$). Furthermore, ZJP-2 markedly reduced DMNQ-induced apoptosis in C17.2 cells. Flow cytometric analysis revealed that DMNQ treatment alone for 24 h resulted in an apoptosis rate of 13.6%, whereas co-treatment with ZJP-2 of 400 μg/mL reduced the apoptotic cell population to 5.98% (Figure 4D–F).

3.6.2. ZJP-2 Attenuates Oxidative Stress via Activation of Antioxidant Pathways

To investigate the antioxidant activity of ZJP-2, intracellular ROS levels were measured following co-treatment of C17.2 cells with DMNQ (3 μM) and ZJP-2 (400 μg/mL) for 24 h. As shown in Figure 5A, DMNQ treatment significantly increased ROS production to approximately 130% compared with the control group ($p < 0.05$), indicating a pronounced oxidative response. Co-treatment with ZJP-2 (400 μg/mL) effectively attenuated this increase, suggesting that ZJP-2 can mitigate redox imbalance and suppress ROS accumulation in neural stem cells.

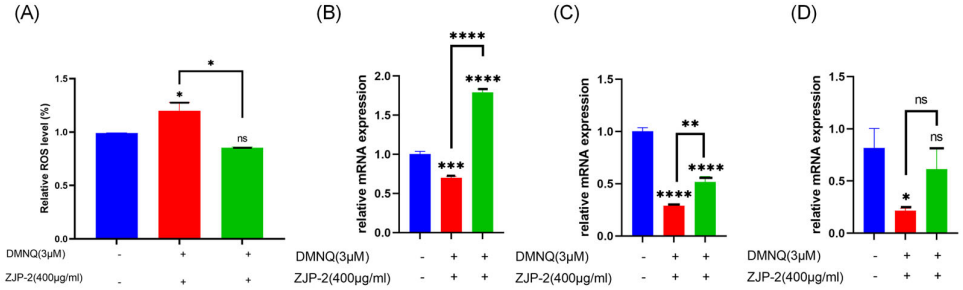

Figure 5. Alleviating effect of ZJP-2 on DMNQ-induced oxidative stress in C17.2 cells. (**A**) Relative intracellular ROS levels in C17.2 cells ($n = 3$). (**B**–**D**) Relative mRNA expression levels of antioxidant genes: (**B**) *HO-1*, (**C**) *Nrf2*, and (**D**) *SOD* ($n = 4$). Data are expressed as mean ± SEM, * $p < 0.05$, ** $p < 0.01$, *** $p < 0.005$, **** $p < 0.001$. vs. Control group (or Model group); ns indicates not significant. Statistical analysis was performed using one-way ANOVA followed by LSD test.

To further investigate the molecular mechanism of this antioxidant activity, real-time PCR analysis was performed to assess the expression levels of antioxidant-related genes. DMNQ treatment resulted in a marked downregulation of *NRF-2*, *HO-1*, and *SOD1* mRNA levels in C17.2 cells. In contrast, ZJP-2 treatment significantly restored or even upregulated the expression of these antioxidant genes ($p < 0.05$) (Figure 5B,C). *HO-1* is a stress-inducible enzyme that can reduce intracellular oxidative stress by decomposing heme, while *SOD1* can catalyze superoxide anions into hydrogen peroxide, thus playing a key role in ROS regulation [47]. Therefore, ZJP-2 may activate the expression of these antioxidant factors and enhance the ability of cells to cope with oxidative stress, thereby exerting a neuroprotective effect.

3.6.3. ZJP-2 Reverses Oxidative Stress-Induced Upregulation of Nestin and NeuN in C17.2 Cells

Under conditions of oxidative stress, the expression of key protein markers in neural cells reflects dynamic changes in cell state and differentiation potential. Nestin is an intermediate filament protein that is widely considered a marker of neural stem and progenitor cells, and its elevated expression is associated with stress-induced activation of endogenous repair mechanisms or a shift to a more primitive proliferative state [48]. In contrast, NeuN (neuronal nucleus, RBFOX3) is a nuclear marker of mature postmitotic neurons, and elevated NeuN levels may reflect stress-related differentiation signals or compensatory responses that promote neuronal maturation [49]. Previous studies have shown that oxidative stress can lead to elevated nestin levels, suggesting that redox imbalance may activate both neural stemness and neuronal differentiation pathways [50]. These changes are indicators of cell adaptation or repair under oxidative conditions.

In this study, the pro-oxidant drug DMNQ was used to induce oxidative stress in C17.2 neural stem cells, and the expression changes in Nestin and NeuN were observed. The results showed that the levels of Nestin and NeuN increased after DMNQ treatment, indicating that redox imbalance may have activated stress-responsive pathways involved in neural stem cell plasticity and neuronal differentiation. After ZJP-2 intervention, the level of oxidative stress was significantly reduced, and the expression of Nestin and NeuN also tended to be adjusted back ($p < 0.05$) (Figure 6A–C). These findings indicate that ZJP-2 helps to maintain neural cell homeostasis and preserves the physiological balance between stemness and differentiation under oxidative conditions [51,52].

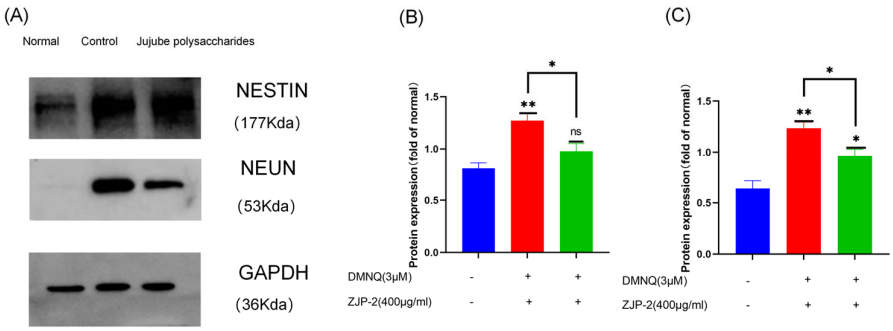

Figure 6. Effects of ZJP-2 on the expression of differentiation-related proteins in DMNQ-treated C17.2 cells. (**A**) Representative Western blot images of Nestin and NeuN. (**B**,**C**) Quantitative analysis of protein expression levels: (**B**) Nestin and (**C**) NeuN. The protein intensity was normalized to the internal control (GAPDH). Data are expressed as mean ± SEM ($n = 3$). * $p < 0.05$, ** $p < 0.01$ vs. Control group (or Model group); ns indicates not significant. Statistical analysis was performed using one-way ANOVA followed by LSD test.

4. Discussion

This study isolated and purified ZJP-2 from Ziziphus jujuba, and systematically characterized its structure using multiple analytical techniques. HPLC-MALS-RI analysis revealed a molecular weight of approximately 67.93 kDa, with a single peak and narrow dispersion, indicating high purity and homogeneity [53]. Combined methylation analysis and NMR revealed that ZJP-2 possesses a typical RG-I backbone composed of (1→4)-α-D-GalA*p*- and (1→2,4)-α-l-Rha*p*-units, bearing structurally defined side chains such as 1,4-Gal*p* and 1,5-Ara*f*, exhibiting a unique regional structural arrangement. We compared it with representative polysaccharides previously reported from different Z. jujuba cultivars. Notably, HJP1 (6.8 kDa) [54] and HJP3 [55] (2.9 kDa) isolated from *cv. Muzao* were characterized as low-molecular-weight, HG-rich pectic fragments dominated by linear homogalacturonan chains. In contrast, ZJP-2 exhibits a moderate molecular weight

(~67.9 kDa) and is RG-I-dominant, indicating a higher degree of structural complexity and side-chain ramification. In addition, ZP2a [56] from *cv. Junzao* (12.1 kDa) was reported as an RG-I polysaccharide bearing arabinan side chains with branching mainly at *O*-3 (e.g., (1→3,5)-α-L-Ara*f* and (1→3)-α-L-Ara*f*). By comparison, our methylation and NMR data demonstrate that the arabinan domain of ZJP-2 contains distinct *O*-2 branching points, characterized by (1→2,5)-α-L-Ara*f* residues, together with galactan segments attached to *O*-4 of rhamnose. This difference in arabinan branching topology ((1→2,5) vs. (1→3,5)) suggests that ZJP-2 may adopt a distinct side-chain conformation and flexibility relative to previously reported jujube RG-I polysaccharides, which could influence polysaccharide–cell interactions and bioactivity. Furthermore, ZJSPs-1 [57] from *cv. Ruoqiangzao* was reported as a very high-molecular-weight polysaccharide (~342 kDa) with incompletely resolved structural features, whereas ZJP-2 shows a well-defined RG-I framework with clearly assigned side-chain linkage patterns. Collectively, these direct comparisons highlight ZJP-2 as a structurally differentiated RG-I-type pectic polysaccharide within the Ziziphus genus.

Recent studies have demonstrated that natural pectin polysaccharides typically exhibit significant neuroprotective effects, functioning through mechanisms such as free radical scavenging, inflammatory response regulation, or modulation of neural plasticity [57]. However, research on wild jujube pectin polysaccharides in the neuroprotective field remains limited. Given ZJP-2's distinctive characteristics in structural assembly, side-chain configuration, and acidity level, its potential neuroactivity warrants investigation. Neural stem cells (NSCs) play a pivotal role in maintaining central nervous system homeostasis and facilitating injury repair [58,59], yet they are highly susceptible to oxidative stress damage. Excessive reactive oxygen species (ROS) impair NSC proliferation, differentiation, and self-renewal capacity, thereby hindering neurogenesis [60]. Establishing an in vitro NSC model eliminates interference from drug metabolism and barrier factors, providing a more direct reflection of polysaccharides' intrinsic antioxidant capabilities [61]. Therefore, validating ZJP-2's biological activity using a DMNQ-induced oxidative damage model in NSCs is a crucial step toward understanding its mechanism of action.

Experimental results demonstrate that ZJP-2 significantly enhances C17.2 cell viability, suppresses apoptosis, and reduces excessive ROS accumulation under oxidative stress conditions, indicating direct cytoprotective effects. Mechanistically, ZJP-2 significantly upregulates the mRNA expression of *Nrf2* and *HO-1*, as well as other antioxidant genes, including *SOD*, thereby enhancing the cell's endogenous free radical scavenging capacity. Concurrently, it reverses the DMNQ-induced abnormal elevation in Nestin and partially restores the expression trend of NeuN, suggesting its potential role in maintaining NSC homeostasis and promoting neural differentiation.

5. Conclusions

In summary, this study systematically elucidates the molecular structure of ZJP-2, an RG-I pectin polysaccharide derived from Ziziphus jujuba, and reveals its antioxidant and neuroprotective mechanisms in a neural stem cell model. As a structurally unique and functionally defined natural polysaccharide, ZJP-2 holds potential application value in developing neuroprotective functional foods and as an adjunct intervention for central nervous system disorders.

Supplementary Materials: The following supporting information can be downloaded at https://www.mdpi.com/article/10.3390/nu18050816/s1; Supplementary Table S1. Molecular characteristic parameters of jujuba polysaccharide ZJP-2; Supplementary Table S2. Monosaccharide analysis data of ZJP-2; Supplementary Figure S1: Protective effect of ZJP-2 on C17.2 cell viability and DMNQ-induced oxidative damage; Supplementary Figure S2: Preliminary screening of ZJP-2 doses on DMNQ-induced intracellular ROS accumulation.

Author Contributions: Conceptualization and Supervision, X.L. and X.Z. (Xing Zhang); Methodology, Investigation, and Formal Analysis, S.L., Q.Z. and N.W.; Validation, N.W. and H.C.; Resources, H.C., N.A. and M.D.; Data Curation and Software, J.L. and X.Z. (Xuchen Zhou); Writing—Original Draft Preparation, S.L.; Writing—Review and Editing, X.L., X.Z. (Xing Zhang) and S.L.; Project Administration and Funding Acquisition, X.L. and X.Z. (Xing Zhang). All authors have read and agreed to the published version of the manuscript. The co-authors finish the proofreading.

Funding: This research was supported by the R&D of Drug and Health Products from Jujube, S&T Department, Xinjiang Government (2023A02010), NGHJG project of Xinjiang Production and Construction Corps (2023AA503), and the Ningbo Top Talent Project (No. 215-432094250), the Health Fund of Translational Biomedicine from Health BioMed Co., Ltd., Ningbo, Zhejiang, China (H2024000279).

Data Availability Statement: The data used in this article cannot be shared widely due to intellectual property considerations. However, specific datasets supporting the findings of this study are available from the corresponding author upon reasonable request. Requests to access the data should be made to Xinmin Liu (liuxinmin@nbu.edu.cn).

Acknowledgments: The authors gratefully acknowledge the funding support from the Xinjiang government (2023A02010), the NGHJG project of Xinjiang Production and Construction Corps (2023AA503), and the Health Fund of Translational Biomedicine (H2024000279). Special thanks to the staff of the Analysis Center in IDDT, Ningbo University for their excellent technical assistance regarding NMR data acquisition, experimental equipment management, and data processing.

Conflicts of Interest: Huabiao Chen was employed by Ningbo Health Gene Technologies Co., Ltd. The remaining authors declare that the research was conducted in the absence of any commercial or financial relationships that could be construed as a potential conflict of interest.

Abbreviations

The following abbreviations are used in this manuscript:

ZJP-2 *Ziziphus jujuba Mill. var. spinosa* (Bunge) Hu ex H. F. Chou polysaccharide-2

References

1. Balkrishna, A.; Sharma, N.; Srivastava, D.; Kukreti, A.; Srivastava, S.; Arya, V. Exploring the safety, efficacy, and bioactivity of herbal medicines: Bridging traditional wisdom and modern science in healthcare. *Future Integr. Med.* **2024**, *3*, 35–49. [CrossRef]
2. Du, S.; Hu, X.; Yang, X.; Yu, W.; Wang, Z. Genetic diversity and population dynamic of *Ziziphus jujuba* var. spinosa (Bunge) Hu ex HF Chow in Central China. *Ecol. Evol.* **2022**, *12*, e9101. [CrossRef] [PubMed]
3. Fu, J.-Y.; Qian, L.-B.; Zhu, L.-G.; Liang, H.-T.; Tan, Y.-N.; Lu, H.-T.; Lu, J.-F.; Wang, H.-P.; Xia, Q. Betulinic acid ameliorates endothelium-dependent relaxation in L-NAME-induced hypertensive rats by reducing oxidative stress. *Eur. J. Pharm. Sci.* **2011**, *44*, 385–391. [CrossRef] [PubMed]
4. Jiang, J.-G.; Huang, X.-J.; Chen, J.; Lin, Q.-S. Comparison of the sedative and hypnotic effects of flavonoids, saponins, and polysaccharides extracted from Semen Ziziphus jujube. *Nat. Prod. Res.* **2007**, *21*, 310–320. [CrossRef]
5. Liu, J.; Qiao, W.; Yang, Y.; Ren, L.; Sun, Y.; Wang, S. Antidepressant-like effect of the ethanolic extract from Suanzaorenhehuan Formula in mice models of depression. *J. Ethnopharmacol.* **2012**, *141*, 257–264. [CrossRef]
6. Park, J.H.; Lee, H.J.; Koh, S.B.; Ban, J.Y.; Seong, Y.H. Protection of NMDA-induced neuronal cell damage by methanol extract of *Zizyphi spinosi* Semen in cultured rat cerebellar granule cells. *J. Ethnopharmacol.* **2004**, *95*, 39–45. [CrossRef]
7. Hua, Y.; Xu, X.-x.; Guo, S.; Xie, H.; Yan, H.; Ma, X.-f.; Niu, Y.; Duan, J.-A.; Chemistry, F. Wild jujube (*Ziziphus jujuba* var. spinosa): A review of its phytonutrients, health benefits, metabolism, and applications. *J. Agric. Food Chem.* **2022**, *70*, 7871–7886. [CrossRef]
8. Benalaya, I.; Alves, G.; Lopes, J.; Silva, L.R. A review of natural polysaccharides: Sources, characteristics, properties, food, and pharmaceutical applications. *Int. J. Biol. Macromol.* **2024**, *25*, 1322. [CrossRef]
9. Lin, T.; Liu, Y.; Lai, C.; Yang, T.; Xie, J.; Zhang, Y. The effect of ultrasound assisted extraction on structural composition, antioxidant activity and immunoregulation of polysaccharides from *Ziziphus jujuba* Mill var. spinosa seeds. *Ind. Crops Prod.* **2018**, *125*, 150–159. [CrossRef]

10. Yue, Y.; Wu, S.; Zhang, H.; Zhang, X.; Niu, Y.; Cao, X.; Huang, F.; Ding, H. Characterization and hepatoprotective effect of polysaccharides from *Ziziphus jujuba* Mill. var. spinosa (Bunge) Hu ex HF Chou sarcocarp. *Food Chem. Toxicol.* **2014**, *74*, 76–84. [CrossRef]
11. Ruan, J.; Han, Y.; Kennedy, J.F.; Jiang, H.; Cao, H.; Zhang, Y.; Wang, T. A review on polysaccharides from jujube and their pharmacological activities. *Carbohydr. Polym. Technol. Appl.* **2022**, *3*, 100220. [CrossRef]
12. Yue, Y.; Wu, S.; Li, Z.; Li, J.; Li, X.; Xiang, J.; Ding, H. Wild jujube polysaccharides protect against experimental inflammatory bowel disease by enabling enhanced intestinal barrier function. *Food Funct.* **2015**, *6*, 2568–2577. [CrossRef] [PubMed]
13. Ji, X.; Peng, Q.; Yuan, Y.; Shen, J.; Xie, X.; Wang, M. Isolation, structures and bioactivities of the polysaccharides from jujube fruit (*Ziziphus jujuba* Mill.): A review. *Food Chem.* **2017**, *227*, 349–357. [CrossRef] [PubMed]
14. Pollock, J.F.; Ashton, R.S.; Rode, N.A.; Schaffer, D.V.; Healy, K.E. Molecular characterization of multivalent bioconjugates by size-exclusion chromatography with multiangle laser light scattering. *Bioconjugate Chem.* **2012**, *23*, 1794–1801. [CrossRef]
15. Wu, X.; Jiang, W.; Lu, J.; Yu, Y.; Wu, B. Analysis of the monosaccharide composition of water-soluble polysaccharides from Sargassum fusiforme by high performance liquid chromatography/electrospray ionisation mass spectrometry. *Food Chem.* **2014**, *145*, 976–983. [CrossRef]
16. Taylor, R.L.; Conrad, H.E. Stoichiometric depolymerization of polyuronides and glycosaminoglycuronans to monosaccharides following reduction of their carbodiimide-activated carboxyl group. *Biochemistry* **1972**, *11*, 1383–1388. [CrossRef]
17. Ciucanu, I.; Kerek, F. A simple and rapid method for the permethylation of carbohydrates. *Carbohydr. Res.* **1984**, *131*, 209–217. [CrossRef]
18. Sims, I.M.; Carnachan, S.M.; Bell, T.J.; Hinkley, S.F. Methylation analysis of polysaccharides: Technical advice. *Carbohydr. Polym.* **2018**, *188*, 1–7. [CrossRef]
19. Shou, J.-W.; Cheung, C.-K.; Gao, J.; Shi, W.-W.; Shaw, P.-C. Berberine protects $C_{17.2}$ neural stem cells from oxidative damage followed by inducing neuronal differentiation. *Front. Cell. Neurosci.* **2019**, *13*, 395. [CrossRef]
20. Xu, J.; Liu, D.; Niu, H.; Zhu, G.; Xu, Y.; Ye, D.; Li, J.; Zhang, Q. Resveratrol reverses Doxorubicin resistance by inhibiting epithelial-mesenchymal transition (EMT) through modulating PTEN/Akt signaling pathway in gastric cancer. *J. Exp. Clin. Cancer Res.* **2017**, *36*, 19. [CrossRef]
21. Alves, M.B.R.; de Andrade, A.; de Arruda, R.; Batissaco, L.; Florez-Rodriguez, S.A.; Lançoni, R.; de Oliveira, B.; Torres, M.A.; Ravagnani, G.M.; de Almeida, T.J.B.P. An efficient technique to detect sperm reactive oxygen species: The CellRox deep red fluorescent probe. *Andrologia* **2015**, *4*, 157.
22. Citri, A.; Pang, Z.P.; Südhof, T.C.; Wernig, M.; Malenka, R.C. Comprehensive qPCR profiling of gene expression in single neuronal cells. *Nat. Protoc.* **2012**, *7*, 118–127. [CrossRef] [PubMed]
23. Hirano, S. Western blot analysis. In *Nanotoxicity*; Humana Press: Totowa, NJ, USA, 2012; pp. 87–97.
24. Guo, Q.; Du, J.; Jiang, Y.; Goff, H.D.; Cui, S.W. Pectic polysaccharides from hawthorn: Physicochemical and partial structural characterization. *Food Hydrocoll.* **2019**, *90*, 146–153. [CrossRef]
25. Wang, Q.; Cui, S.W. Understanding the physical properties of food polysaccharides. *Food Carbohydr. Chem. Phys. Prop. Appl.* **2005**, *1*, 162–214.
26. Bellich, B.; Distefano, M.; Syrgiannis, Z.; Bosi, S.; Guida, F.; Rizzo, R.; Brady, J.W.; Cescutti, P. The polysaccharide extracted from the biofilm of Burkholderia multivorans strain C1576 binds hydrophobic species and exhibits a compact 3D-structure. *Int. J. Biol. Macromol.* **2019**, *136*, 944–950. [CrossRef]
27. Zhao, Y.; Li, P.; Wang, X.; Wu, Y.; Liu, L.; Zhao, R. A novel pectin polysaccharide from vinegar-baked Radix Bupleuri absorbed by microfold cells in the form of nanoparticles. *Int. J. Biol. Macromol.* **2024**, *266*, 131096. [CrossRef]
28. Liu, Y.; Meng, Y.; Ji, H.; Guo, J.; Shi, M.; Lai, F.; Ji, X. Structural characteristics and antioxidant activity of a low-molecular-weight jujube polysaccharide by ultrasound assisted metal-free Fenton reaction. *Food Chem.* **2024**, *24*, 101908. [CrossRef]
29. Zhang, G.; Liu, C.; Zhang, R. A novel acidic polysaccharide from blackened jujube: Structural features and antitumor activity in vitro. *Front. Nutr.* **2022**, *9*, 1001334. [CrossRef]
30. Ciucanu, I. Per-O-methylation reaction for structural analysis of carbohydrates by mass spectrometry. *Anal. Chim. Acta* **2006**, *576*, 147–155. [CrossRef]
31. Zhang, M.; Wang, G.; Lai, F.; Wu, H. Structural characterization and immunomodulatory activity of a novel polysaccharide from Lepidium meyenii. *J. Agric. Food Chem.* **2016**, *64*, 1921–1931. [CrossRef]
32. Hong, T.; Zhao, J.; Yin, J.; Nie, S.; Xie, M. Structural characterization of a low molecular weight HG-type pectin from Gougunao green tea. *Front. Nutr.* **2022**, *9*, 878249. [CrossRef] [PubMed]
33. Yapo, B.M. Rhamnogalacturonan-I: A structurally puzzling and functionally versatile polysaccharide from plant cell walls and mucilages. *Polym. Rev.* **2011**, *51*, 391–413. [CrossRef]
34. Mikshina, P.V.; Gurjanov, O.P.; Mukhitova, F.K.; Petrova, A.A.; Shashkov, A.S.; Gorshkova, T.A. Structural details of pectic galactan from the secondary cell walls of flax (*Linum usitatissimum* L.) phloem fibres. *Carbohydr. Polym.* **2012**, *87*, 853–861. [CrossRef] [PubMed]

35. Smestad Paulsen, B.; Barsett, H. Bioactive pectic polysaccharides. In *Polysaccharides I*; Springer: Berlin/Heidelberg, Germany, 2005; pp. 69–101.
36. Ji, X.; Cheng, Y.; Tian, J.; Zhang, S.; Jing, Y.; Shi, M. Structural characterization of polysaccharide from jujube (*Ziziphus jujuba* Mill.) fruit. *Chem. Biol. Technol. Agric.* **2021**, *8*, 54. [CrossRef]
37. Lin, X.; Liu, K.; Yin, S.; Qin, Y.; Shen, P.; Peng, Q. A novel pectic polysaccharide of jujube pomace: Structural analysis and intracellular antioxidant activities. *Antioxidants* **2020**, *9*, 127. [CrossRef]
38. Yan, S.; Liu, X.; Wang, Y.; Yang, X.; Bai, L.; Sun, L.; Zhou, Y.; Cui, S. Structural characterization and antioxidant activity of pectic polysaccharides from *Veronica peregrina* L. *Front. Nutr.* **2023**, *10*, 1217862.
39. He, F.; Zhang, S.; Li, Y.; Chen, X.; Du, Z.; Shao, C.; Ding, K. The structure elucidation of novel arabinogalactan LRP1-S2 against pancreatic cancer cells growth in vitro and in vivo. *Carbohydr. Polym.* **2021**, *267*, 118172. [CrossRef]
40. Zhang, H.; Yue, Y.; Zhang, Q.; Liang, L.; Li, C.; Chen, Y.; Li, W.; Peng, M.; Yang, M.; Zhao, M. Structural characterization and anti-inflammatory effects of an arabinan isolated from *Rehmannia glutinosa* Libosch. *Carbohydr. Polym.* **2023**, *303*, 120441. [CrossRef]
41. Cui, Y.; Wang, R.; Cao, S.; Ismael, M.; Wang, X.; Lü, X. A galacturonic acid-rich polysaccharide from Diospyros kaki peel: Isolation, characterization, rheological properties and antioxidant activities in vitro. *Food Chem.* **2023**, *416*, 135781. [CrossRef]
42. Lin, P.; Wang, Q.; Wang, Q.; Chen, J.; He, L.; Qin, Z.; Li, S.; Han, J.; Yao, X.; Yu, Y. Evaluation of the anti-atherosclerotic effect for Allium macrostemon Bge. Polysaccharides and structural characterization of its a newly active fructan. *Carbohydr. Polym.* **2024**, *340*, 122289. [CrossRef]
43. Butt, H.S.; Ulriksen, E.S.; Rise, F.; Wangensteen, H.; Duus, J.Ø.; Inngjerdingen, M.; Inngjerdingen, K.T. Structural elucidation of novel pro-inflammatory polysaccharides from *Daphne mezereum* L. *Carbohydr. Polym.* **2024**, *324*, 121554.
44. Wang, J.; Zhou, Y.; Yu, Y.; Wang, Y.; Xue, D.; Zhou, Y.; Li, X. A ginseng-derived rhamnogalacturonan I (RG-I) pectin promotes longevity via TOR signalling in Caenorhabditis elegans. *Carbohydr. Polym.* **2023**, *312*, 120818. [CrossRef] [PubMed]
45. Huo, J.; Lei, M.; Li, F.; Hou, J.; Zhang, Z.; Long, H.; Zhong, X.; Liu, Y.; Xie, C.; Wu, W. Structural characterization of a polysaccharide from gastrodia elata and its bioactivity on gut microbiota. *Molecules* **2021**, *26*, 4443. [CrossRef] [PubMed]
46. Monks, T.J.; Jones, D.C. The metabolism and toxicity of quinones, quinonimines, quinone methides, and quinone-thioethers. *Curr. Drug Metab.* **2002**, *3*, 425–438. [CrossRef] [PubMed]
47. Sies, H.; Belousov, V.V.; Chandel, N.S.; Davies, M.J.; Jones, D.P.; Mann, G.E.; Murphy, M.P.; Yamamoto, M.; Winterbourn, C. Defining roles of specific reactive oxygen species (ROS) in cell biology and physiology. *Nat. Rev. Mol. Cell Biol.* **2022**, *23*, 499–515. [CrossRef]
48. Park, D.; Xiang, A.P.; Mao, F.F.; Zhang, L.; Di, C.-G.; Liu, X.-M.; Shao, Y.; Ma, B.-F.; Lee, J.-H.; Ha, K.-S. Nestin is required for the proper self-renewal of neural stem cells. *Stem Cells* **2010**, *28*, 2162–2171. [CrossRef]
49. Duan, W.; Zhang, Y.-P.; Hou, Z.; Huang, C.; Zhu, H.; Zhang, C.-Q.; Yin, Q. Novel insights into NeuN: From neuronal marker to splicing regulator. *Mol. Neurobiol.* **2016**, *53*, 1637–1647. [CrossRef]
50. Richter-Landberg, C.; Goldbaum, O. Stress proteins in neural cells: Functional roles in health and disease. *Cell. Mol. Life Sci.* **2003**, *60*, 337–349. [CrossRef]
51. Sahlgren, C.M.; Pallari, H.M.; He, T.; Chou, Y.H.; Goldman, R.D.; Eriksson, J.E. A nestin scaffold links Cdk5/p35 signaling to oxidant-induced cell death. *EMBO J.* **2006**, *25*, 4808–4819. [CrossRef]
52. Cheng, C.-Y.; Su, S.-Y.; Tang, N.-Y.; Ho, T.-Y.; Chiang, S.-Y.; Hsieh, C.-L. Ferulic acid provides neuroprotection against oxidative stress-related apoptosis after cerebral ischemia/reperfusion injury by inhibiting ICAM-1 mRNA expression in rats. *Brain Res.* **2008**, *1209*, 136–150. [CrossRef]
53. Zhang, X.; Li, L.; Fung, H.; Chen, N.; Shan, P.; Zhou, Y.; Han, Q. Critical review of the criterion of polysaccharide purity. *Carbohydr. Polym.* **2025**, *352*, 123187. [CrossRef] [PubMed]
54. Wang, Y.; Liu, X.; Zhang, J.; Liu, G.; Liu, Y.; Wang, K.; Yang, M.; Cheng, H.; Zhao, Z. Structural characterization and in vitro antitumor activity of polysaccharides from *Zizyphus jujuba* cv. Muzao. *RSC advances. RSC Adv.* **2015**, *5*, 7860–7867. [CrossRef]
55. Li, J.; Ai, L.; Yang, Q.; Liu, Y.; Shan, L. Isolation and structural characterization of a polysaccharide from fruits of Zizyphus jujuba cv. Junzao. *Int. J. Biol. Macromol.* **2013**, *55*, 83–87. [CrossRef] [PubMed]
56. Wu, Z.; Li, H.; Wang, Y.; Yang, D.; Tan, H.; Zhan, Y.; Yang, Y.; Luo, Y.; Chen, G. Optimization extraction, structural features and antitumor activity of polysaccharides from *Z. jujuba* cv. *Ruoqiangzao* seeds. *Int. J. Biol. Macromol.* **2019**, *135*, 1151–1161. [CrossRef]
57. Gao, Q.-H.; Fu, X.; Zhang, R.; Wang, Z.; Guo, M. Neuroprotective effects of plant polysaccharides: A review of the mechanisms. *Int. J. Biol. Macromol.* **2018**, *106*, 749–754. [CrossRef]
58. Galli, R.; Gritti, A.; Bonfanti, L.; Vescovi, A.L. Neural stem cells: An overview. *Circ. Res.* **2003**, *92*, 598–608. [CrossRef]
59. Shi, Y.; Sun, G.; Zhao, C.; Stewart, R. Neural stem cell self-renewal. *Crit. Rev. Oncol. Hematol.* **2008**, *65*, 43–53. [CrossRef]

60. Niedzielska, E.; Smaga, I.; Gawlik, M.; Moniczewski, A.; Stankowicz, P.; Pera, J.; Filip, M. Oxidative stress in neurodegenerative diseases. *Mol. Neurobiol.* **2016**, *53*, 4094–4125. [CrossRef]
61. Wang, Z.-J.; Xie, J.-H.; Nie, S.-P.; Xie, M.-Y. Review on cell models to evaluate the potential antioxidant activity of polysaccharides. *Food Funct.* **2017**, *8*, 915–926. [CrossRef]